Chapter 10

Silicon-on-Insulator Slot Waveguides: Theory and Applications in Electro-Optics and Optical Sensing

Patrick Steglich

Additional information is available at the end of the chapter

http://dx.doi.org/10.5772/intechopen.75539

Abstract

This chapter deals with the basic concept of silicon-on-insulator (SOI) slot waveguides, including slot waveguide theory, fabrication steps, and applications. First, in the theory section, a modal field expression and the characteristic equation is derived, which is also valid for higher-order modes. SOI slot waveguide structures are simulated and characteristic values like the effective refractive indices and the field confinement factors are determined. The fabrication section describes typical SOI fabrication steps and the limits of current fabrication techniques. Additionally, developments regarding loss reduction in SOI slot waveguides are given from the fabrication point of view. This is followed by the theory and practice of slot waveguide based electro-optical modulators. Here, the SOI slot waveguide is embedded in an organic nonlinear optical material in order to achieve record-low voltage-length products. In the field of optical sensors, it is shown that slot waveguides enable remarkable waveguide sensitivity for both refractive index sensing and surface sensing.

Keywords: silicon-on-insulator (SOI), slot waveguide, polymer-based optical waveguides, silicon-organic hybrid waveguide, optical waveguides technology, electro-optic waveguides, waveguide sensing

1. Introduction

Recent developments in cloud computing, social media, and the Internet of things have heightened the need for integrated photonic communication systems. To compensate for the emerged data traffic, electro-optical (EO) modulators with large bandwidth and high-speed operation are necessary. This in turn needs novel material systems and waveguide structures since the established depletion-type modulators are speed limited due to carrier injection and

removal. In contrast, polymer-based EO modulators exhibit high-speed operation but suffer from process compatibility with the well-established silicon-on-insulator (SOI) technology, which makes high volume and cheap production challenging.

After the invention by Almeida et al. in 2004 [1], slot waveguides became one key element to combine the well-established SOI technology with nonlinear optical polymers [2]. In recent years, there has been an increasing interest in slot waveguide structures. An SOI slot waveguide consists of a small gap in between two silicon rails, where a nonlinear optical polymer can be deposited. This narrow gap has two effects. First, the guided light is partly confined inside the gap. Second, the gap leads to an extremely large electric field, while voltages as low as 1 V are applied. Consequently, a record-high operation speed and large bandwidth with low energy consumption has been demonstrated using the silicon-organic hybrid (SOH) photonics [3].

Researchers have also discovered the advantages of slot waveguides for optical sensing. In this case, the slot waveguide takes advantage from the fact that more than 70% of the guided light can be confined near the silicon rails. Therefore, the light has a stronger interaction with the analyte compared to common strip waveguides, where only a fraction, 20%, of the light can be interacting. This strong light-analyte interaction leads to a large waveguide sensitivity, which has pushed the development of recent integrated optical sensors.

This work examines the theory and applications of SOI slot waveguides for EO modulators and optical sensors. We provide a theoretical guideline for a deeper understanding of SOI slot waveguides. The present work is structured as follows. The following section focuses on a detailed theoretical description and analysis of slot waveguide structures. This is followed by a section on the fabrication scheme using standard SOI technology. Finally, application notes in electro-optics and optical sensing are given in Sections 4 and 5, respectively.

2. Silicon-on-insulator slot waveguide

This section deals with the basic concepts of SOI slot waveguides. For a deeper understanding of slot waveguide structure, the breakthrough paper of Almeida et al. [1] is recommended. However, the modal field expression given in [1] has some transcription errors and the given characteristic equation is not explicit for solving higher-order modes. Therefore, the correct modal field expression and the characteristic equation, which is also valid for higher-order modes is provided in this chapter, following the comprehensive work of Liu et al. [4].

2.1. Introduction to silicon-on-insulator waveguides

In general, silicon waveguides can be readily fabricated from SOI wafers using standard CMOS (complementary metal-oxide-semiconductor) processes. A typical SOI wafer consists of a buried oxide (BOX) layer between the silicon wafer and a thin silicon layer. Optical lithography and etching techniques are used to form the silicon waveguide. The most common silicon waveguide is the strip waveguide. This waveguide has a rectangular geometry as

http://dx.doi.org/10.5772/intechopen.75539

shown in **Figure 1**. During the last decade, a new waveguide approach based on vertical silicon slot waveguides has been proposed [1] and experimentally demonstrated to be suitable as an optical phase shifter [2]. An SOI slot waveguide consists typically of two silicon rails with a height of $h = 220$ nm. This thickness of 220 nm has become a standard used in particular by most multi-project wafer foundries [5]. As illustrated in **Figure 1**, both silicon rails are located on top of a buried oxide (BOX) substrate and are separated from each other by a slot width s. The width of the silicon rails is denoted as wg. Slot waveguides enable a high field confinement in a narrow low-index region. Infiltration of the interior of the slot waveguide with an EO polymer allows the use of the Pockels effect. Because of this effect, slot wave guides have high potential in the field of optical switching and high-speed modulation even at frequencies of 100 GHz [3]. As a consequence, various devices like Mach-Zehnder interferometers and ring resonators have been recently developed using slot waveguide phase shifters [6]. In fact, slot waveguides have become the key element in order to implement organic materials into silicon photonics. Beside the strip and slot waveguide, the strip-loaded slot waveguide is utilized in this work. The cross section of each waveguide type is shown in **Figure 1**.

The overwhelming advantage of SOI slot waveguides lies in its compatibility with CMOS fabrication processes. This compatibility ensures a cost efficient mass production environment for such integrated photonic devices. **Figure 2** shows, as an example, a scanning electron microscopy (SEM) picture of three slot waveguides with different slot widths from the top view and one slot waveguide in the cross-sectional view recorded with a focused ion beam (FIB). They were fabricated in an SiGe BiCMOS pilot line at the Institute of High-Performance Microelectronics (IHP) in Frankfurt (Oder) using 200 mm SOI wafers and 248 nm lithography.

2.2. Silicon-on-insulator slot waveguide theory

One major advantage of slot waveguides compared to strip waveguides is the fact that the guided light is partially confined in between two silicon rails. Consequently, the light is forced

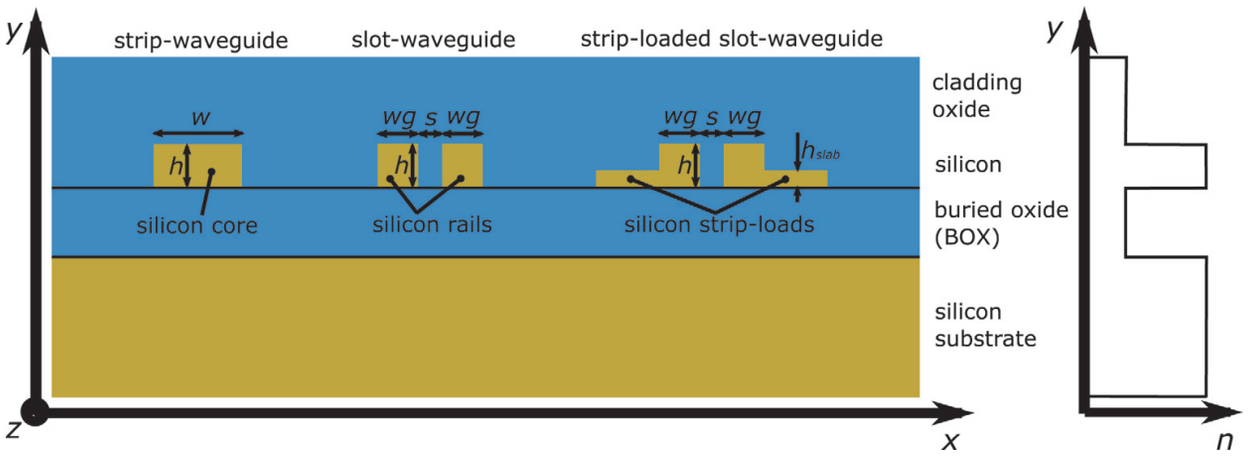

Figure 1. Typical silicon-on-insulator waveguide types. The most common waveguide type is the strip waveguide, where the light is highly confined inside the silicon core. In case of slot waveguides, the light is confined near two silicon rails. To apply a voltage to the silicon rails, strip-loads serve as electrical connections. The corresponding waveguide is called a strip-loaded slot waveguide.

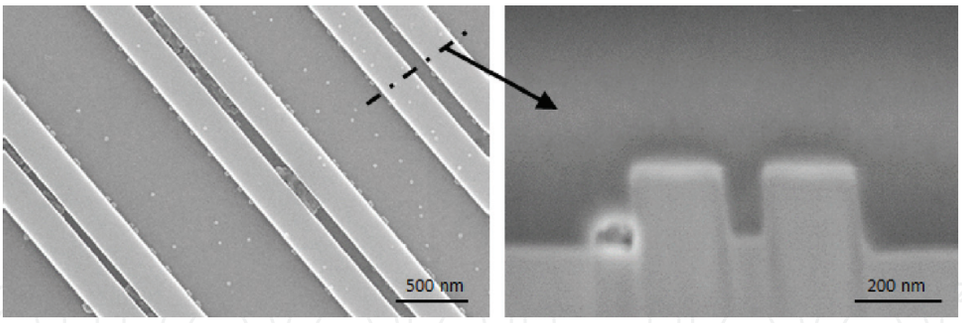

Figure 2. SEM image (left) of slot waveguides with different slot widths fabricated using 248 nm lithography. FIB image (right) of a slot waveguide cross section [13].

to interact directly with the cladding material. The reason for the high confinement is the large index contrast of the high-index silicon n_{si} and the low-index cladding material n_{clad}. At the interface the normal electric field, which is according to **Figure 1**, the E_x field component, undergoes a large discontinuity. This results in a field enhancement in the low-index region, which is proportional to the ratio of the refractive indices of the cladding material to that of silicon,

$$E_{x,slot} = \frac{n_{si}^2}{n_{clad}^2} E_{x,si} \tag{1}$$

Here, $E_{x,slot}$ and $E_{x,si}$ represent the electric field inside the slot and inside the silicon, respectively. From Eq. (1), it is apparent that the modal field distribution in the slot depends on the quotient of the refractive indices of silicon and the slot material. The larger the n_{si} to n_{clad} ratio, the stronger is the normal electric field component in the slot. Considering silicon with a refractive index of 3.48 and air as cladding material with a refractive index of 1.0, the resulting field amplitude is more than 12 times higher in the slot region according to Eq. (1). The high confinement inside the slot is of special benefit for EO and biosensing applications.

As shown in **Figure 2**, a conventional slot waveguide structure with finite height consists of two rectangle silicon rails. In the following, we will transform the three-dimensional (3D) rectangular silicon rails of the slot waveguide into a two-dimensional (2D) slab waveguide, where the height of the slot waveguide becomes infinite as illustrated in **Figure 3**. The coordinate system is set in the center of the slab-based slot waveguide. This slab waveguide approximation makes it easier to find an analytical solution and is simpler and more intuitive than numerical methods like the finite element method (FEM).

For the E_x component of the fundamental TM (transverse magnetic) mode, the Helmholtz equation for each layer becomes

$$\frac{d^2E_x}{dx^2} + \left[k_0^2 n^2(x) - \beta^2\right] E_x = 0, \tag{2}$$

where

http://dx.doi.org/10.5772/intechopen.75539

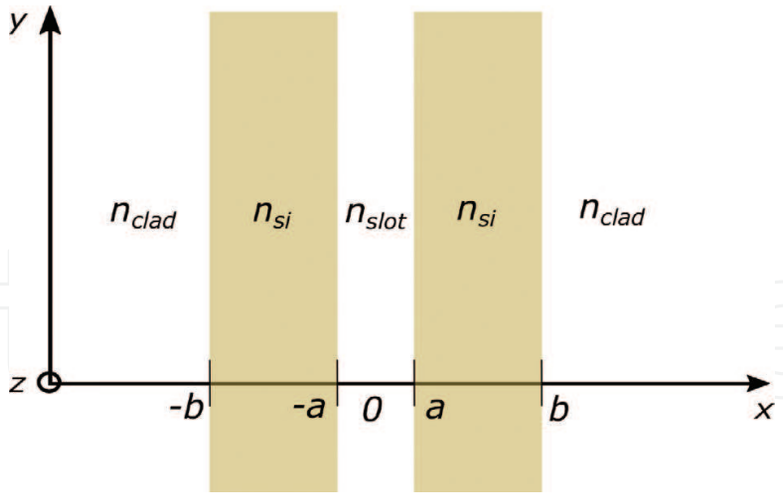

Figure 3. Schematic of the slot waveguide structure with infinite height (slab waveguide approximation). The refractive index of the slot is denoted as n_{slot}.

$$n(x) = f(x) = \begin{cases} n_{slot}, & if\ |x| < a \\ n_{si}, & if\ a < |x| < b \\ n_{clad}, & if\ |x| > b \end{cases} \tag{3}$$

and $\beta = k_0 n_{eff}$ denotes the mode propagation constant with the effective refractive index n_{eff}. Letting

$$\gamma_{slot}^2 = \beta^2 - k_0^2 n_{slot}^2 \tag{4}$$

$$\gamma_{si}^2 = k_0^2 n_{si}^2 - \beta^2 \tag{5}$$

$$\gamma_{clad}^2 = \beta^2 - k_0^2 n_{clad}^2 \tag{6}$$

the Helmholtz equation can be expressed as

$$\begin{cases} \dfrac{d^2 E_x}{dx^2} - \gamma_{slot}^2 E_x = 0, & if\ |x| < a \\ \dfrac{d^2 E_x}{dx^2} + \gamma_{si}^2 E_x = 0, & if\ a < |x| < b \\ \dfrac{d^2 E_x}{dx^2} - \gamma_{clad}^2 E_x = 0, & if\ |x| > b \end{cases} \tag{7}$$

The effective refractive index is obtained by solving the Eigen equation of the waveguide structure. In case of the TM fundamental mode, the following condition is assumed: $n_{si} > n_{clad} \geq n_{slot}$. The analysis of other cases like $n_{si} > n_{slot} > n_{clad}$ is out of the scope of this thesis. For a more detailed analysis the work of Liu et al. [4] is recommended. However, by choosing reasonable modal field functions in each layer of the slab-based slot waveguide and

employing the electromagnetic field boundary conditions, the modal field solution and the characteristic equation can be obtained. In consideration of the natural boundary condition and waveguide symmetry the general solution for the transverse E-field profile E_x of the fundamental TM mode is

$$E_x(x) = \begin{cases} A_1 \cosh\left(\gamma_{slot} x\right), & if\ |x| < a \\ A_2 \cos\left(\gamma_{si}|x|\right) + B_2 \sin\left(\gamma_{si}|x|\right), & if\ a < |x| < b \\ A_3 e^{-\gamma_{clad}|x|}, & if\ |x| > b \end{cases} \tag{8}$$

Here, A_1, A_2, A_3 and B_2 are constants. Assuming that there is no free charge at the boundary, the boundary continuous conditions for the TM mode are the continuity of the normal component of the electric displacement field $\left(n_{clad}^2 E_{x,clad} = n_{si}^2 E_{x,si}\right)$ and $\left(n_{slot}^2 E_{x,slot} = n_{si}^2 E_{x,si}\right)$ and the continuity of dE_x/dx. At boundary surfaces $|x| = a$ and $|x| = b$, the boundary continuous conditions are used to derive the coefficients and the eigenvalue equation for β. The eigenvalue equation is a transcendental equation and is given by

$$\tan^{-1}\left(\frac{n_{si}^2}{n_{clad}^2}\frac{\gamma_{clad}}{\gamma_{si}}\right) + \tan^{-1}\left(\frac{n_{si}^2}{n_{slot}^2}\frac{\gamma_{slot}}{\gamma_{si}}\tanh\left(\gamma_{slot} a\right)\right) + m{\cdot}\pi = \gamma_{si}(b-a) \tag{9}$$

where m is an integer. The analytical solution of the fundamental TM mode is obtained by substituting the coefficients into the general solution for E_x (Eq. (8)), which leads to the modal field expression

$$E_x(x) = A\begin{cases} \dfrac{1}{n_{slot}^2}\cosh\left(\gamma_{slot} x\right), & if\ |x| < a \\ \dfrac{1}{n_{si}^2}\cosh\left(\gamma_{slot} a\right)\cos\left(\gamma_{si}(|x| - a)\right) & \\ + \dfrac{1}{n_{slot}^2}\dfrac{\gamma_{slot}}{\gamma_{si}}\sinh\left(\gamma_{slot} a\right)\sin\left(\gamma_{si}(|x| - a)\right), & if\ a < |x| < b \\ \dfrac{1}{n_{clad}^2}\left(\cosh\left(\gamma_{slot} a\right)\cos\left(\gamma_{si}(b-a)\right)\right. & \\ \left. + \dfrac{n_{si}^2}{n_{slot}^2}\dfrac{\gamma_{slot}}{\gamma_{si}}\sinh\left(\gamma_{slot} a\right)\sin\left(\gamma_{si}(b-a)\right)\right)e^{-\gamma_{clad}|x|}, & if\ |x| > b \end{cases} \tag{10}$$

where A is an arbitrary constant. As an example, **Figure 4** shows the normalized E_x field distribution of a typical silicon slot waveguide. This figure gives an evidence of the large discontinuity and the high E-field confinement inside the slot region.

2.3. Simulation of slot waveguides

In this section, a commercial full-vectorial finite element method (FEM) based mode solver from COMSOL Multiphysics is employed to simulate the slot waveguide structure with finite height.

http://dx.doi.org/10.5772/intechopen.75539

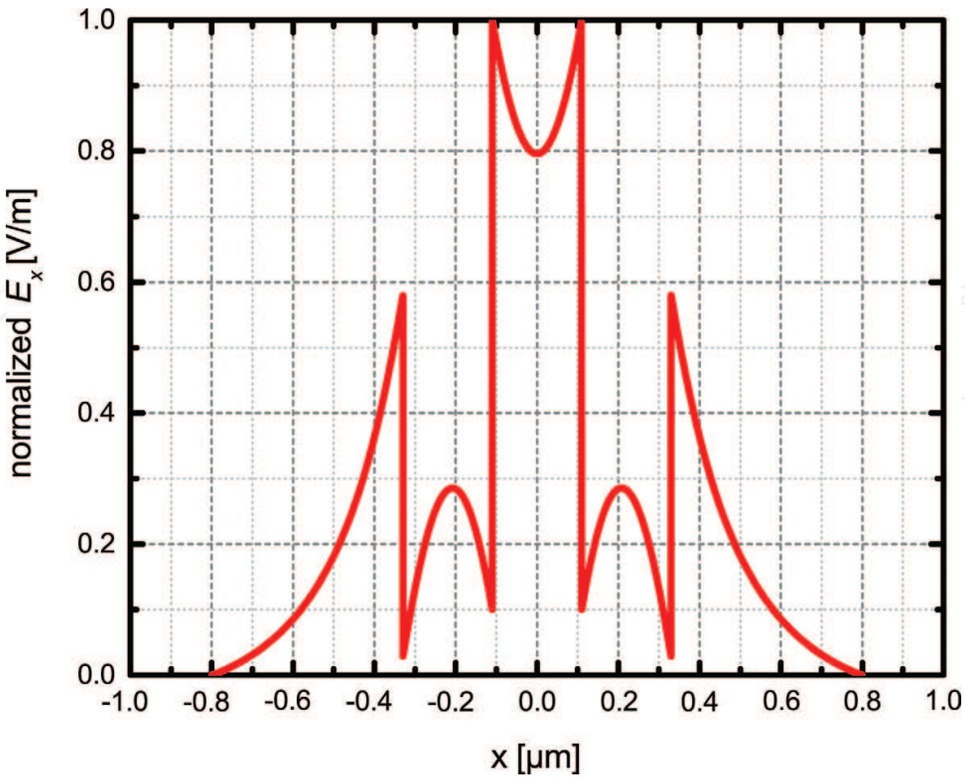

Figure 4. Calculated E_x field (normalized) for a slot waveguide structure with infinite height. Parameters: $\lambda = 1550$ nm, $a = 110$ nm, $b = 220$ nm, $n_{slot} = n_{clad} = 1.44$, $n_{si} = 3.48$.

Here, the quasi-TE eigenmode presents the major E-field component along the x-direction [1]. Consequently, the quasi-TE eigenmode in the 3D slot waveguide structure is analogous to the TM eigenmode in the slab-based slot waveguide structure, which was studied in the previous section. In the following simulation study, the waveguide parameters, i.e., the silicon rail width *wg* and the slot width *s*, are variable whereas the height *h* is fixed to 220 nm (see **Figure 5**).

The wavelength is assumed to be $\lambda = 1550$ nm because it is a typical telecommunication wavelength in silicon photonics. Triangular vector elements with a maximum and minimum

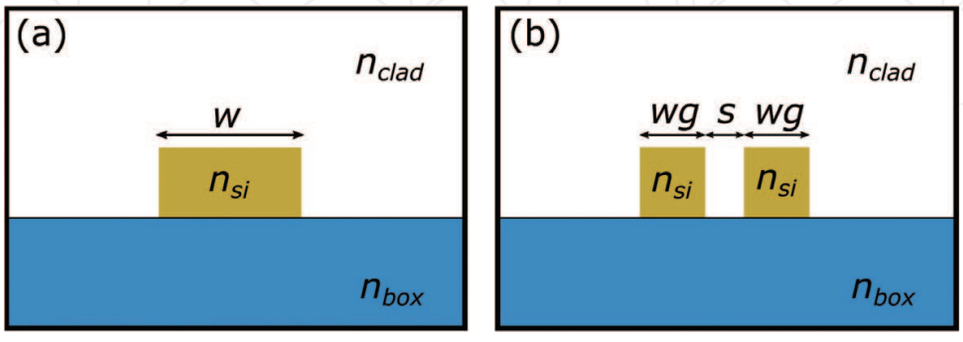

Figure 5. Cross-sectional view of an SOI strip waveguide (a) and an SOI slot waveguide (b). The cladding oxide is removed to hybridize the silicon waveguide with an EO polymer (EO modulator) or to bring the waveguide in contact with an analyte (biochemical sensor). The refractive indices are denoted as n_{clad}, n_{si} and n_{box} for the caldding material, silicon and buried oxide substrate, respectively.

element size of 6 and 2 nm, respectively have been adopted for meshing the profile with over 1.2×10^4 mesh elements. The overall simulation area was $3 \times 3\ \mu m$. In order to yield the mode field distribution and effective refractive index, the refractive index distribution $n(x, y)$ need to be declared to calculate eigenvalues and eigenfunctions of the wave equation. Finally, we get the E-field intensity distribution for the quasi-TE and quasi-TM mode as shown in **Figure 6**. In the following, we will neglect the quasi-TM mode because it is over two orders of magnitude smaller than the quasi-TE mode.

The material properties for our simulations were taken from a Sellmeier fit of the optical data from Malitson (SiO_2) [16] and Salzberg and Villa (Si) [17], which corresponds to having $n_{SiO_2} = n_{box} = 1.444$ and $n_{si} = 3.48$ at $\lambda = 1550$ nm. The refractive index of the surrounding material is in general variable because it can be gas, fluid or solid, depending on the application. For exemple, we chose $n_{clad} = 1.7$, which corresponds to a commercially available and reliable organic material named M3 (commercialized by GigOptix Inc.). M3 is successfully used for several slot waveguide based EO modulators like in [2, 18–20].

As result, the effective refractive index can be obtained from this simulation. **Figure 7** shows the calculated effective refractive indices n_{eff} as a function of the slot width s and the rail width wg. From this figure, it can be seen that the effective refractive index becomes higher by increasing the rail width wg and by decreasing the slot width s. Therefore, such parameters have to be taken into account in order to design slot waveguide based mode coupler, ring resonators, or similar photonic components.

2.4. SOI slot waveguide optimization

In order to design and improve the waveguide geometry for applications in the field of EO modulators and optical sensors, it is necessary to calculate characteristic values, which describe the optical field confinement and therefore the interaction of light with the surrounding material.

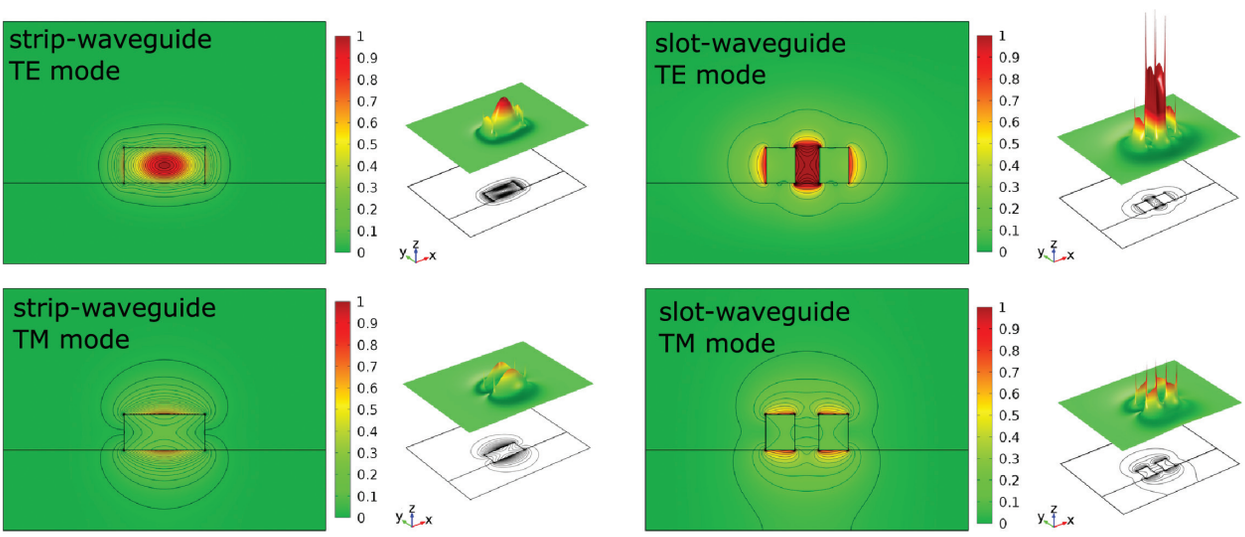

Figure 6. FEM simulation of the normalized E-field intensity $|E_x|^2 + |E_y|^2 + |E_z|^2$ for the first TE and first TM mode of SOI strip and slot waveguides. Parameters: $\lambda = 1550$ nm, $n_{box} = 1.444$, $n_{si} = 3.48$.

http://dx.doi.org/10.5772/intechopen.75539

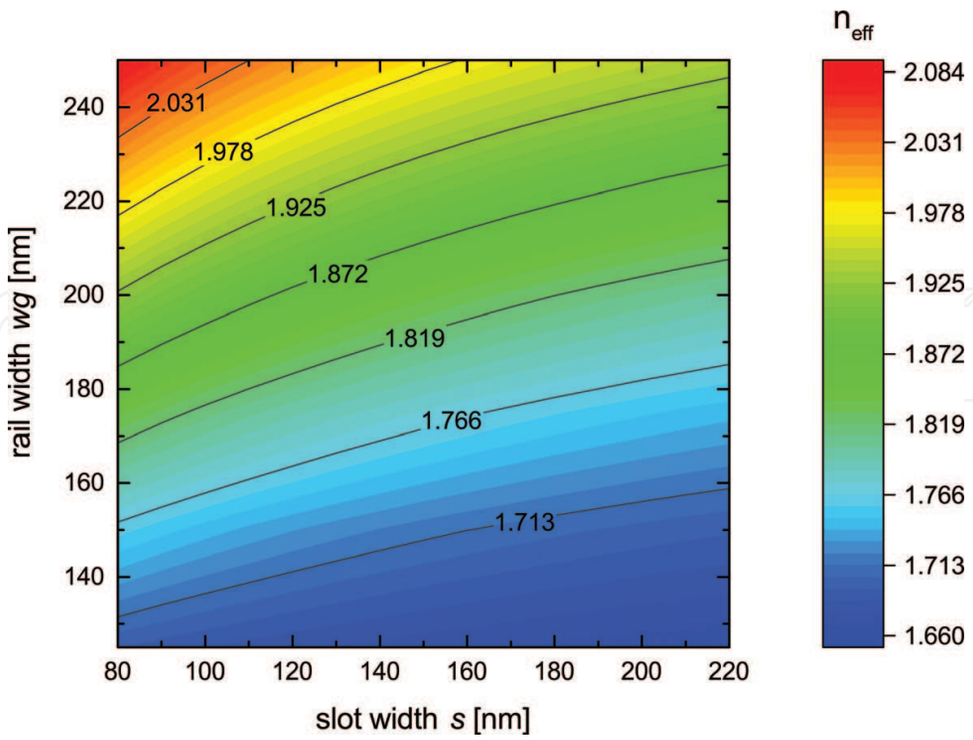

Figure 7. Calculated effective refractive indices n_{eff} of SOI slot waveguides as a function of the slot width s and the rail width wg.

One key figure of merit is the field confinement factor. In particular, it describes how well the guided modal field is confined in a certain region and is defined as the ratio of the time averaged energy flow through the domain of interest (D_{int}) to the time averaged energy flow through the total domain (D_{tot})

$$\Gamma = \frac{\iint_{D_{int}} \mathrm{Re}\{E \times H^*\} e_z dxdy}{\iint_{D_{tot}} \mathrm{Re}\{E \times H^*\} e_z dxdy} \tag{11}$$

Here, E and H are the electric and magnetic field vectors, respectively, and e_z is the unit vector in the z direction. There are four different cases in order to choose the domain of interest, as illustrated in **Figure 8**. In case of common strip waveguides for electro-optics, the domain of interest is usually equal to the core region ($D_{int} = D_{core}$) because high confinement inside the core leads to lower optical losses. In contrast to that, for bio-sensing applications, the region of the cladding region is considered to be the domain of interest ($D_{int} = D_{clad}$), which is valid for strip and slot waveguides as well. The reason for this is that the main goal is to have a high light interaction with the surrounding material. Considering slot waveguides for electro-optics, the domain of interest is equal to the slot region ($D_{int} = D_{slot}$). There is also a change in refractive index outside the slot since the electric field is also located outside. This contribution is, however, very small compared to that one inside the slot if we assume the linear EO effect (Pockels effect). The Pockels effect requires indeed a non-centro-symmetrical orientation of the EO polymers or non-centro-symmetric organic crystals. Because of that, the main part of the electric field, which gives a contribution to the refractive index change, is the x-component.

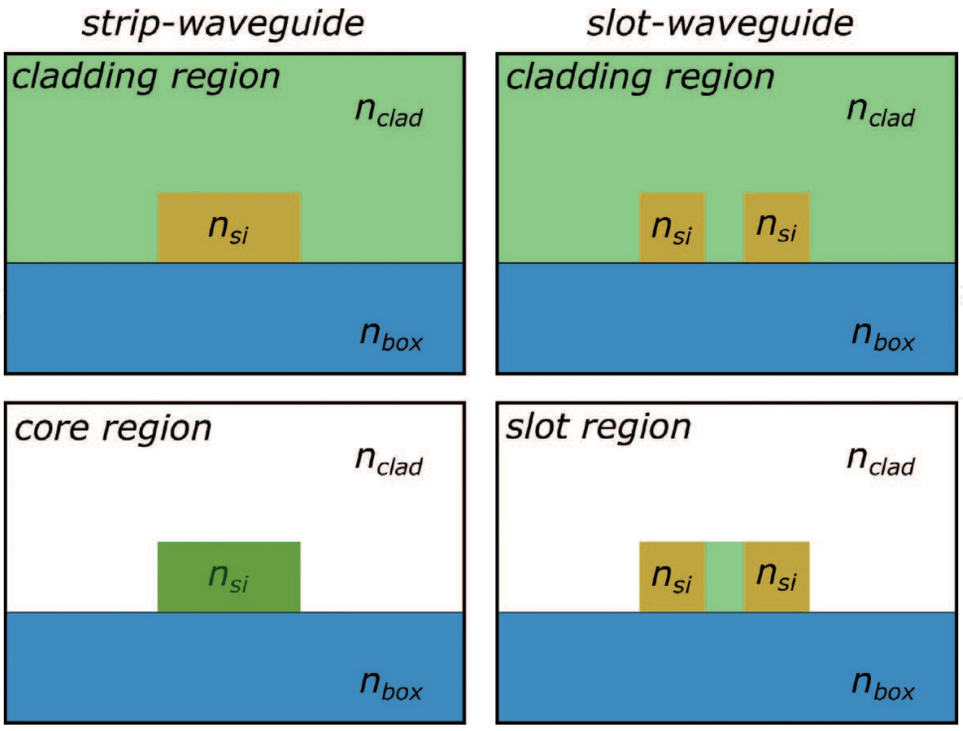

Figure 8. Domains of interest: core D_{core}, cladding D_{clad} and slot D_{slot} regions are highlighted in green. Please note that the substrate is not included in the cladding region because it does not contribute to the electro-optical or sensing effect. Only the amount of light, which is interacting with the cladding material, i.e. in the cladding or in the slot region, is of interest.

The x-component is homogeneous inside the slot. Outside there is just a little projection of the x-component which contributes as shown in **Figure 9**. This figure shows a simulation of the optical and electrical field in case of a strip-loaded slot waveguide. The strip-load serves as the electrical contact. In the following, however, the field confinement factor will be determined for slot waveguides without strip-load; the results are also valid for strip-loaded slot waveguides since the difference is negligible.

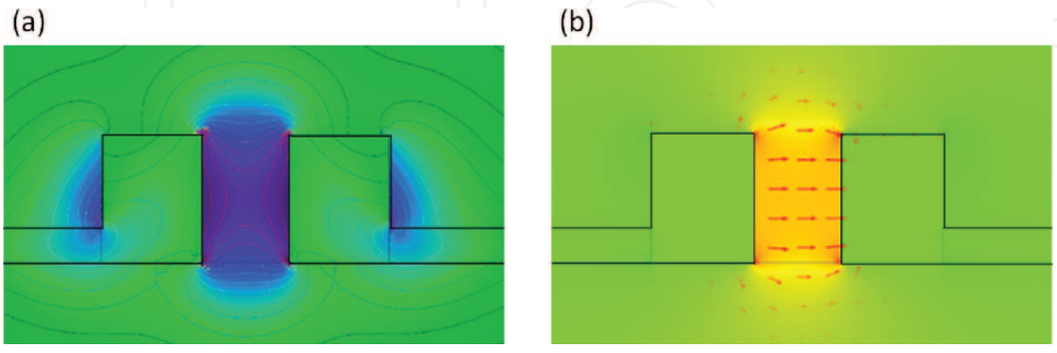

Figure 9. (a) The normalized optical field distribution for the quasi-TE eigenmode of a strip-loaded slot waveguide structure and (b) normalized x-component of the electric field (E_x). The largest overlap between optical and electrical field is achieved inside the slot. Because of that, Pockels effect outside the slot region is negligible and therefore, the field confinement factor in the slot region Γ_{slot} should be taken into account in order to avoid an underestimation of the refractive index change Δn.

http://dx.doi.org/10.5772/intechopen.75539

To validate our simulation approach and compare it with literature data, the field confinement factors of standard SOI strip waveguides are investigated additionally and depicted in **Figure 10**. The domains of interest are the silicon core and the cladding in this case. Note that the substrate is not included in the calculated domains and, therefore, the sum of the core and cladding field confinement factor is not equal to unity. As can be seen from **Figure 10**, there is a large confinement of about 0.76 in the silicon core region of a strip waveguide with a typical waveguide width of $w = 500$ nm. These results are in good agreement with the literature [7].

However, to maximize the sensitivity of SOI slot waveguide based biochemical sensors, it is necessary to maximize the field confinement factor of the cladding (which will be referred to as Γ_{clad}) in order to increase the light-analyte interaction. From **Figure 11**, it can be seen that the confinement in the cladding region of a slot waveguide is increased by decreasing the rail width wg and increasing the slot width s. We chose this parameter range to be compatible with typical semiconductor production platforms. For $wg = 180$ nm, the highest confinement in the cladding region is obtained in the parameter range of our simulation. For a slot waveguide with $wg = 180$ nm and $s = 180$ nm we obtain a field confinement factor of $\Gamma_{clad} = 0.69$. This is an enhancement of about five times compared to a conventional strip waveguide with a typical waveguide width of $w = 500$ nm. With that result, the high sensitivity of slot waveguide based label-free sensors as stated by Claes et al. can be explained [8]. However, due to the difficulty in functionalizing the interior of the slot, the sensitivity could be smaller than expected.

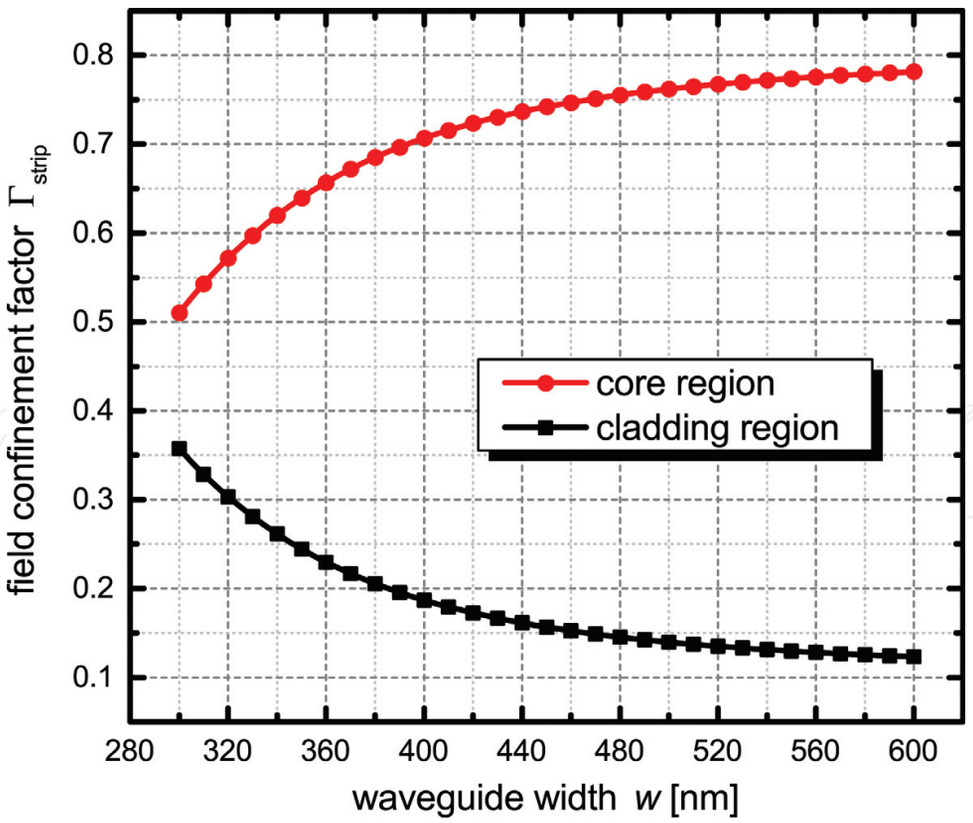

Figure 10. Calculated field confinement factor Γ_{strip} of conventional SOI strip waveguides for the core and cladding region as a function of the waveguide width wg.

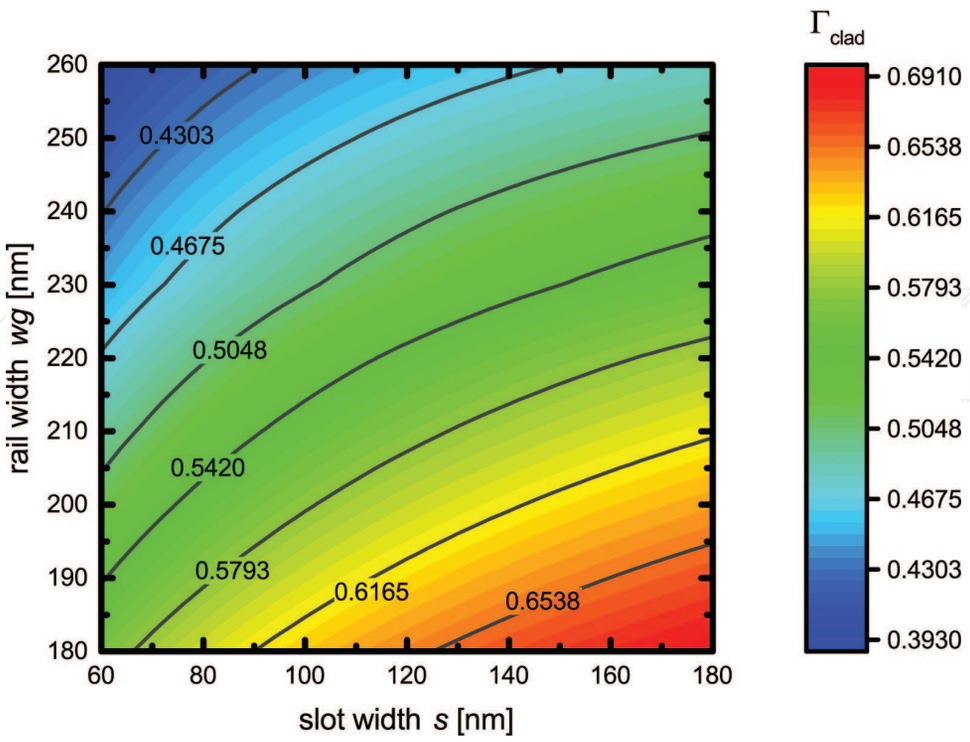

Figure 11. Calculated field confinement factor Γ_{clad} of an SOI slot waveguide for the cladding region in dependence on the slot width s and the rail width wg.

In order to improve SOI slot waveguides for EO applications, it is necessary to find the highest confinement in the slot region. **Figure 12** shows the calculated field confinement factors for the slot region Γ_{slot} as a function of the slot width s and the rail width wg as parameter. As can be seen from this figure, there is one maximum of the highest field confinement of $\Gamma_{slot} = 0.216$ at a slot width of $s = 116$ nm and a rail width of $wg = 200$ nm. This is about three times smaller compared to an SOI strip waveguide (see **Figure 10**). However, in this case, it is more convenient to relate the field confinement factor Γ_{slot} to the area where the light is confined as figure of merit, $\xi_{slot} = \Gamma_{slot}/A_{slot}$ and $\xi_{clad} = \Gamma_{clad}/A_{clad}$. In our case, A_{slot} is equal to the slot domain of the slot waveguide and A_{strip} is equal to the silicon core domain of the strip waveguide. For the optimized slot waveguide structure ($s = 116$ nm, $wg = 200$ nm), this figure of merit is about $\xi_{slot} = 7.83 \times 10^{12}\ \mathrm{m}^{-1}$ and for a typical strip waveguide ($w = 500$ nm), it is about $\xi_{slot} = 6.82 \times 10^{12}\ \mathrm{m}^{-1}$. Even ξ_{slot} is 15% higher than ξ_{strip}; one should keep in mind that a modulator with extremely high field confinement usually suffers very high optical loss. This off-loss can make any modulator useless. With the calculated field confinement factor, an underestimation of the required interaction length for an EO phase modulator is ensured, but such estimation might lead to a field confinement factor that looks prohibitive for using such modulators. The key benefit of slot waveguides is nevertheless the use of organic materials with EO coefficients that are more than one order of magnitude higher compared to semiconductors like GaAs or strained silicon.

http://dx.doi.org/10.5772/intechopen.75539

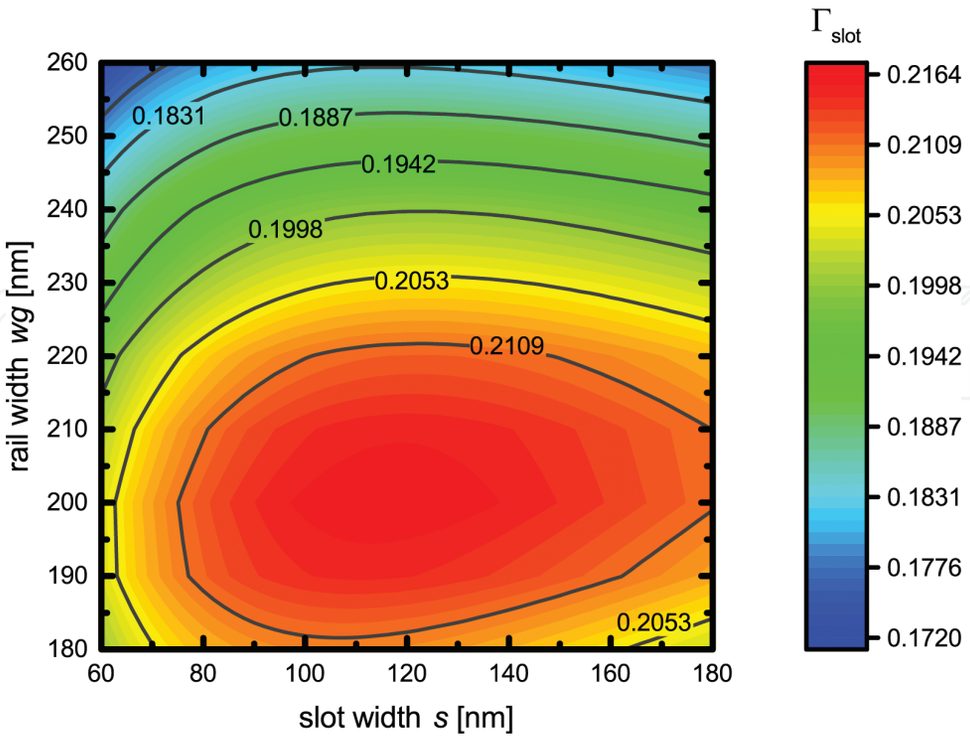

Figure 12. Calculated field confinement factor Γ_{slot} of an SOI slot waveguide for the slot region as a function of the slot width s and the rail width wg.

3. Fabrication of silicon-on-insulator slot waveguides

After the physical layout is developed and simulated, the optimized design need to be converted to a chip layout. Then the fabrication can be realized in an SOI pilot line. This section describes a typical process flow, which can be used with a 200 mm SOI wafer and 248 nm optical lithography or electron beam lithography. Commonly, SOI slot waveguides are fabricated by optical lithography, which enables slot width in the range of 120 nm to 200 nm. To reduce the slot width it is possible to use electron beam lithography.

The complete fabrication scheme is illustrated in **Figure 13**. The basis is an SOI wafer with a 220 nm silicon layer on top of a 2 μm buried oxide layer. In fact, the silicon layer is the actual waveguide layer. It can be doped in a certain area (**Figure 13a–c**) with boron in order to reduce electric conductivity. In this case, the boron doping concentration is about 10^{17} cm^{-3} and, hence, the resulting conductivity is about 11.3 $\Omega^{-1}cm^{-1}$. Then, the waveguide is reduced to create thin slabs, which will be used as the electric connection from the electrodes to the slot waveguide (**Figure 13d–e**). This is followed by etching the slot down until the substrate (**Figure 13f–h**). It is essential to etch it completely because a connection between both silicon rails would lead to a current flow, which in turn induces heat. To further reduce the electric conductivity, another doping step with higher boron doping concentration needs to be performed, as illustrated in **Figure 13i–k**. This higher doping area is placed a few hundreds

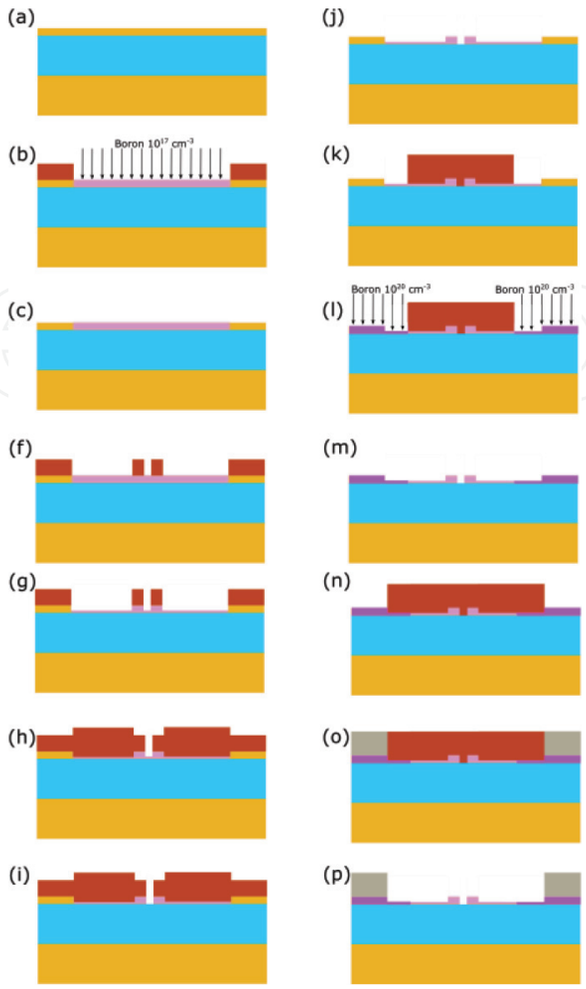

Figure 13. Schematic representation of the fabrication flow of a silicon-on-insulator slot waveguide.

of nanometers away from the slot waveguide (for example, 800 nm) to avoid optical losses due to two photon absorption and free carrier absorption. The boron doping concentration is 10^{20} cm^{-3} and, hence, the resulting conductivity is about 1177.86 Ω^{-1}cm^{-1}. Finally, the electric contacts are formed by depositing aluminum on the doped silicon (**Figure 13i–n**). A silicide intermediate layer can be used between the aluminum and doped silicon in order to reduce the resistivity.

However, only a few SOI slot waveguide-based ring resonators are published so far. The main reason for this fact is that slot-waveguide structures suffer from relatively high losses, mainly caused by sidewall roughness [24]. As a consequence, slot waveguide resonators like micro-ring resonators have typically small optical quality factors (Q-factors). One possible approach to tackle this problem is to reduce propagation losses in the slot waveguides by atomic layer deposition of thin dielectric films, for example, amorphous titanium dioxide (TiO_2) [25, 26]. This reduces, on the one hand, propagation losses but on the other hand, it is associated with additional and not economical production steps, which makes it rather unattractive from the commercial point of view. Another way to tackle this problem is to improve the coupling efficiency. For example, an improvement of 10 times mechanical, thermal the optical Q-factor was demonstrated recently [27].

http://dx.doi.org/10.5772/intechopen.75539

4. Electro-optic modulation in slot waveguides

Electro-optic modulators based on slot waveguides typically examine the linear EO effect, also known as Pockels effect, in organic materials such as organic crystals or polymers. In general, an EO polymer consists of a passive matrix of polymer chains that gives the material its mechanical, thermal, and chemical stability. This matrix is doped with active molecules that have a strong Pockels effect. Most EO devices based on organic EO materials use dipolar molecules embedded in or covalently attached to polymeric material lattices. A device-relevant EO activity requires a macroscopic non-centrosymmetric orientation, which is usually achieved by electric field poling of molecules endowed with their own lack of symmetry. This leads to a linear EO effect, which is appropriated for high-frequency applications.

The linear EO effect in terms of the refractive index change Δn can be determined by

$$\Delta n = -\frac{1}{2} n_{eop}^3 rE = \frac{1}{n_{eop}} \chi^{(2)} E, \tag{12}$$

where n_{eop} represents the refractive index of the EO polymer, r is the linear EO coefficient, E is the electric field, and $\chi^{(2)}$ denotes the second-order susceptibility. In SOI slot waveguides, the electric field can be determined by $E = U/s$, where U is the applied voltage. Comparing the coefficients in Eq. (12) gives the relation between linear EO coefficient and second-order susceptibility

$$r = -\frac{2\chi^{(2)}}{n_{eop}^4}. \tag{13}$$

The linear EO coefficient r describes the EO activity of a centrosymmetric material and can be represented by [9].

$$r \propto N\beta \left\langle \cos^3 \theta \right\rangle \tag{14}$$

Here, N is the chromophore number density or the number of nonlinear molecules in the material contributing to the polarization, β represents the molecular first hyperpolarizability, and $\left\langle \cos^3 \theta \right\rangle$ denotes the average non-centrosymmetric order parameter.

θ denotes the angle between molecular dipole axis and the electric field vector. Eq. (14) suggests strategies to increase the linear EO effect:

1. Increasing the chromophore number density N.
2. Using chromophores with high first hyperpolarizability β.
3. Maximizing the average non-centrosymmetric order parameter $\left\langle \cos^3 \theta \right\rangle$ by inducing a high molecular orientation.

Such requirements are best met by EO polymers which are dipolar and exhibit a highly polarizable donor-π-acceptor (D-π-A) system. This D-π-A system can support a charge transfer between electron donating and electron withdrawing groups [10]. For electron donating

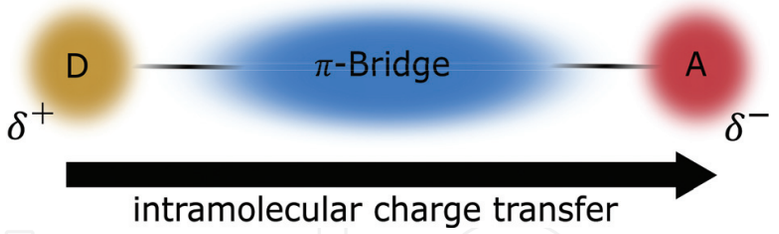

Figure 14. D-π-a system. EO polymers are typically composed of electron donating (D) and electron accepting (A) side groups.

usually the following side groups are used: $N(CH_3)_2$, OCH_3, OH, while for electron accepting groups the following ones: NO, O_2N, CHO, CN. The π-electron conjugated segment serves to transmit the charge, as illustrated in **Figure 14**.

In this work, we demonstrate EO modulation in an SOI slot waveguide using the azobenzene dye Disperse Red 1 doped in poly(methyl methacrylate). This guest-host polymer system is infiltrated into the slot waveguide by spin-coating. A ring resonator is employed to demonstrate intensity modulation. Here, the slot waveguide is partially introduced in the ring. The geometry values are the same as in our previous work in Ref. [11]. This ring resonator has been recently shown to operate efficiently as EO switch [12] and is fabricated in a SiGe BiCMOS pilot line on a 200 nm SOI wafer at the Institute of Innovative Microelectronics IHP in Frankfurt (Oder), Germany. This work, however, demonstrates intensity modulation by applying a function generator to the ground-signal-ground electrodes instead of a DC source. For this experiment, an external cavity laser operating the optical C-band is used as light source, which is polarized to obtain a quasi TE mode in the slot waveguide. A schematic of the complete experimental set-up is shown in **Figure 15**. For our demonstration, we applied a sine signal with a peak-to-peak voltage of 1 V at a frequency of 25 kHz. The oscilloscope traces in **Figure 16** show the applied electrical

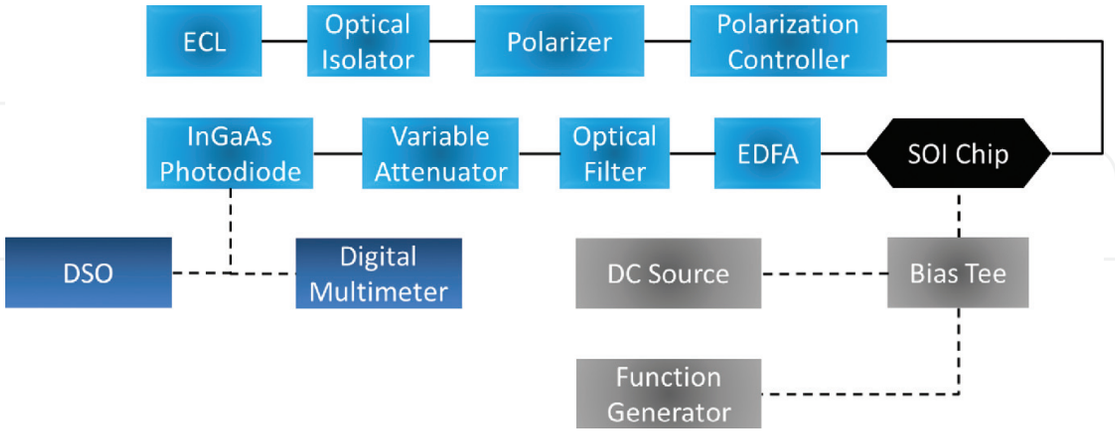

Figure 15. Schematic of the experimental set-up for EO modulation. An external cavity laser (ECL) is polarized and coupled to the SOI chip. An erbium doped fiber amplifier (EDFA) is used to amplify the outcoupled light. A 2 nm optical filter is applied to avoid signal noise from the EDFA and a variable attenuator is used to avoid damaging the InGaAs photodetector. Finally, the modulated signal is recorded with a digital sampling oscilloscope (DSO). The digital multimeter was used for wavelength adjustment.

http://dx.doi.org/10.5772/intechopen.75539

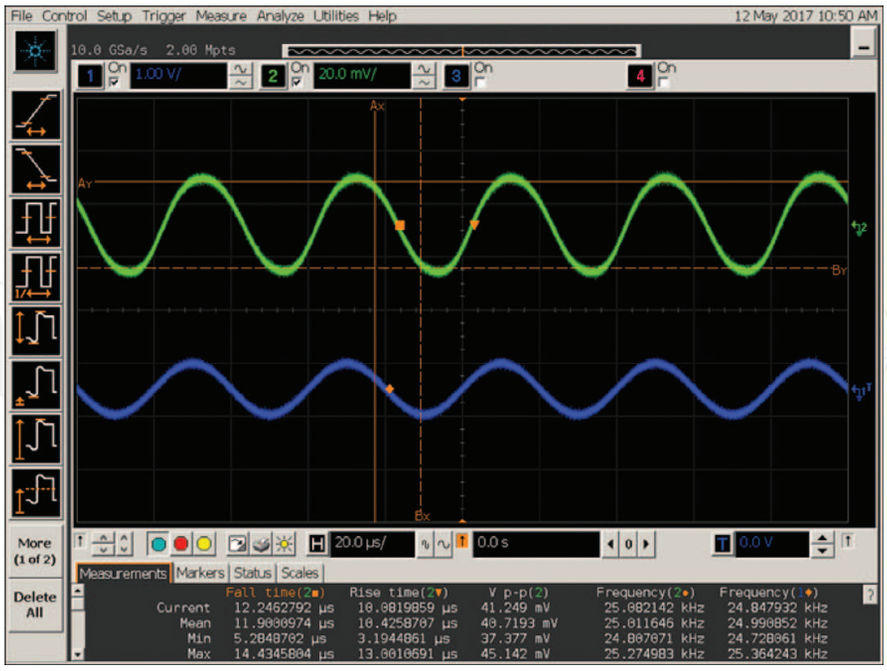

Figure 16. Oscilloscope traces of the electrical sine signal (blue) and the modulated optical signal (green). The peak-to-peak voltage of the electrical signal is 1 V and the modulation frequency is 25 kHz.

signal (blue) and the observed optical signal (green). The present experiment demonstrates the feasibility of a polymer filled SOI slot waveguide for EO modulation at low voltages. It is worthwhile to note that the applied voltage of 1 V is compatible with common CMOS-based drivers; making the present approach attractive from the commercial point of view.

5. Optical sensing in slot waveguides

The working principle of photonic ring resonators for biochemical sensing is based on refractive index sensing, i.e., the measurement of the resonance wavelength shift $\Delta\lambda$ due to a refractive index change Δn_s of the solution containing the analyte in specific concentration. This refractive index change is typically subjected to a change in concentration. In order to measure the resonance wavelengths, the light of a tunable laser is in-coupled to the photonic chip out-coupled via an optical fiber, and detected by a photodiode. According to the resonance conditions, only selected wavelengths can propagate in the ring and distinct resonance peaks appear in the output spectrum.

In principle, the resonant wavelength λ_{res} of the device depends on the effective refractive index n_{eff} of the optical waveguide that, in turn, is determined by the refractive index of the analyte. Therefore, by detecting changes in the resonant wavelength $\Delta\lambda$ of the ring, small changes in refractive index Δn_s of the solution can be determined. The wavelength shift can be calculated by [13].

$$\Delta\lambda = \frac{\lambda_{res}}{n_g}\Delta n_s \Gamma_{clad}, \tag{15}$$

where Γ_{clad} is the field confinement factor in the cladding which has to satisfy the condition $\Delta n_{eff} = \Gamma_{clad} n_s$.

Generally, there are two types of sensing mechanisms, namely homogenous sensing and surface sensing, that a ring resonator can perform. The difference is the origin of sensing signal as shown in **Figure 17**. Homogeneous sensing signals results from the refractive index change induced by the presence of the analytes in the whole region of the evanescent field, which leads to a non-specific measurement. Detection of chemicals, for example, 2-propanol, sodium

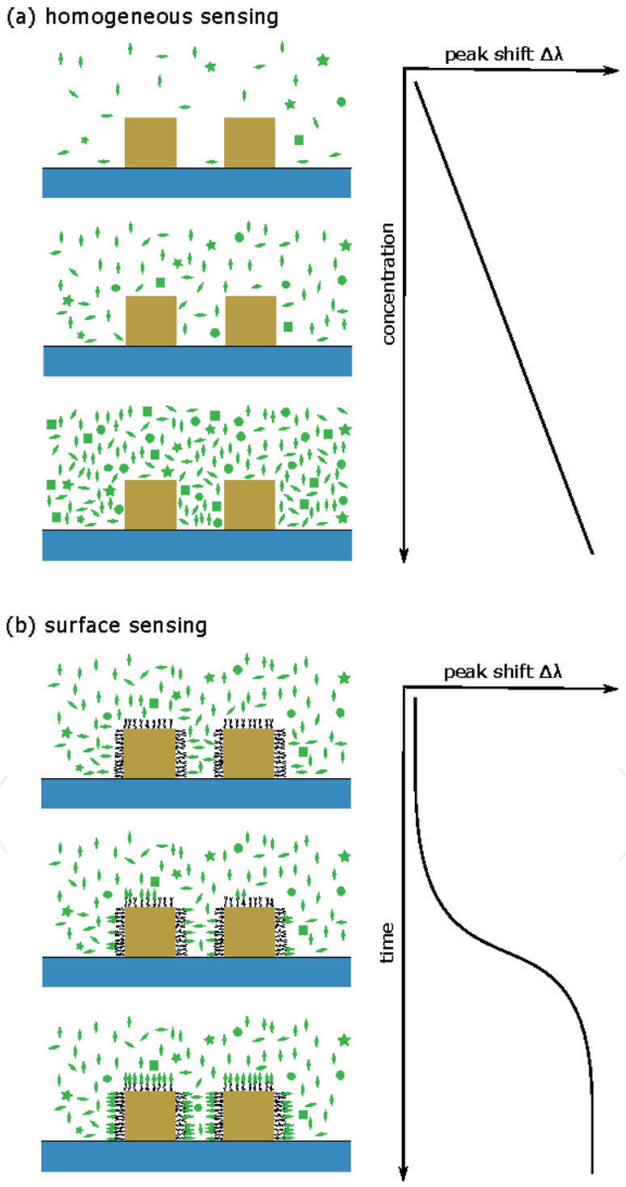

Figure 17. Schematic of the surface sensing principle. The cross section shows that the receptor molecules (antibody) are located on top of slot waveguide surface. The resonance peak is shifted due to a specific binding event. From this data the quantity of the adsorbed analyte is obtained.

http://dx.doi.org/10.5772/intechopen.75539

chloride, and ethylene glycol, has been demonstrated using homogenous sensing [14]. However, homogeneous sensing usually lacks detection specificity.

In contrast, surface sensing signals originate from analytes in the close vicinity of the ring resonator surface [14]. In this case, the surface of the silicon waveguide is modified with an antibody. Only specific analytes can be attached to the antibody, i.e., this analyte-antibody binding leads to a specific measurement. Once the analyte-antibody binding takes place, the residuals can be removed by drying or flushing to enhance the specific measurement. When the antigen, for example, proteins or DNA, interacts with the antibody, the optical wave is influenced in its propagation, the resonance condition changes, and the resonance peak shifts by $\Delta\lambda$. The magnitude of the wavelength shift $\Delta\lambda$ provides information on the quantity of the adsorbed analyte, where the detection limit of the sensor is defined by the minimum resolvable wavelength shift. Moreover, by measuring the peak wavelength shift during the binding process, the binding kinetic can be observed.

However, the main advantage of SOI slot waveguides is the fact that more light can interact with the analyte. A possible explanation for this is the large field confinement factor in the cladding region [15]. This fact leads to an enhanced waveguide sensitivity defined as

$$S_{wg} = \frac{\delta n_g}{\delta n_s}. \tag{16}$$

The waveguide sensitivity, however, does not take into account the resonant structure of widely used ring resonators. Therefore, a second sensitivity is defined as the ring resonator sensitivity given by

$$S_{rr} = \frac{\delta \lambda_{res}}{\delta n_s}. \tag{17}$$

SOI slot waveguide based ring resonators have been demonstrated to achieve more than three times larger ring resonator sensitivities compared to conventional strip waveguide based ring resonators [8]. Notwithstanding this, slot waveguide based ring resonators have not been yet translated into a large overall sensitivity since the optical losses increase the detection limit described by the full width at half maximum (*FWHM*). At large *FWHM* the resonance peak shift may not be resolved. To take both into account (ring resonator sensitivity and the *FWHM*), we can define a figure of merit *FOM* given by

$$FOM = \frac{S_{rr}}{FWHM}. \tag{18}$$

However, the experimental demonstration of surface sensing is beyond the scope of this work, as it needs sophisticated surface modification techniques. Instead, this work focuses on homogenous sensing and demonstrates an exemplary detection of 2-propanol to prove the feasibility of the novel ring resonator concept. This demonstration has the aim of verifying that the concept has practical potential.

We will now turn to the experimental demonstration of homogeneous sensing. To validate our theoretical investigations we fabricated a hybrid-waveguide ring resonator with an SiGe

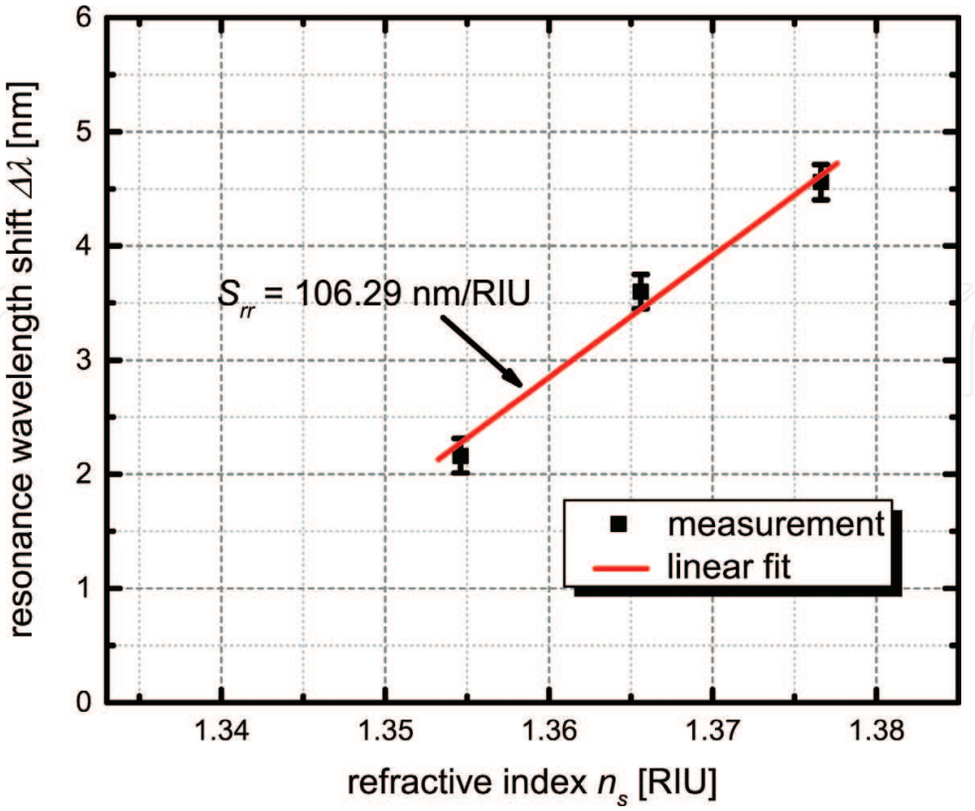

Figure 18. Measured resonance wavelength shift versus refractive index of the test liquid (100, 75, and 50% 2-propanol in deionized water). The slope of the linear fit gives the resonator sensitivity of $S_{rr} = 106.29$ nm/RIU [21].

BiCMOS pilot line. The slot width of the fabricated device is $s = 150$ nm and the rail width is $wg = 180$ nm. A comprehensive study and all geometric parameters of the hybrid-waveguide ring resonator can be found in Ref. [21].

As preliminary test, we measured 100, 75 and 50% concentrations of 2-propanol in de-ionized water. The test liquids are directly dropped onto the surface of the sensor. The refractive indices of the liquids were independently measured by means of a refractometer (Kern ORT 1RS) obtaining 1.3766, 1.3656, and 1.3546 for 100, 75, and 50%, respectively, in good agreement with literature values [22, 23]. **Figure 18** shows the resonance wavelength shift $\Delta\lambda$ versus refractive index n_s of the liquid solutions [21]. Each measurement is carried out five times to prove reproducibility. Regression analysis was used to predict the ring resonator sensitivity. A ring resonator sensitivity of $S_{rr} = 106.29$ nm/RIU and a *FOM* of 1337 were observed. For comparison, a strip waveguide-based ring resonator has typically a ring resonator sensitivity of about 70 nm/RIU and a *FOM* of 903. This result demonstrates the feasibility of SOI slot waveguides for biochemical sensing and the advantage in terms of sensitivity with respect to SOI strip waveguides.

6. Summary

In conclusion, this work has theoretically and experimentally studied aspects of SOI slot waveguides. Simulation and analysis of SOI slot waveguides have been carried out using a

http://dx.doi.org/10.5772/intechopen.75539

finite element method based mode solver. We have determined field confinement factors for the slot and cladding region for applications as EO modulator and optical sensor, respectively. According to the present simulation study, SOI slot waveguides provide about five times higher field confinement in the cladding region with respect to conventional SOI strip waveguides. These results can be used for design optimizations in order to achieve optimum SOI slot waveguide dimensions for sensing applications.

The present study was designed to determine the optical and electro-optical characteristics of SOI slot waveguide-based devices. The presented hybrid-waveguide ring resonator consisting of a slot waveguide implemented in a strip waveguide-based ring resonator has a set of characteristics, which makes it an excellent and unique candidate for low power switches and modulators in the field of optical communication systems. The device was fabricated using CMOS fabrication processes, which enables high integration density and scalable, large-volume manufacturing. One of the more significant findings to emerge from this study is the significantly improved EO response compared to common ring-based modulators making use of the plasma dispersion effect, giving rise to the perspective of sub-femtojoule EO switching. In addition, we have performed intensity modulation at 25 kHz. So far, these characteristics are not combined in any other ring resonator to our knowledge. Moreover, there is still significant room for enhancing the device performance in terms of EO response, for example, by taking advantage of the continuously improving EO polymers. Taken together, the presented results suggest that the slot waveguide-based ring resonators are promising candidates for future EO switches, modulators and tunable filters. Future work should investigate the poling procedure to achieve a larger linear EO effect and therefore, higher modulation frequencies using the same EO polymer. Another limitation is the utilized EO polymer. Using advanced EO polymers indicate that the current results could be further improved. Notwithstanding these limitations, the device performance observed in this study indicate the great promises of using EO polymers which are essential for various hybrid photonic devices particularly for low-power applications. The demonstrated ring resonator opens a new route toward promising applications in the realm of polymer-based non-linear photonics.

A further aspect investigated in this work was the use of SOI slot waveguides for optical sensing. As proof of principle, homogeneous sensing of different concentrations of 2-propanol in de-ionized water was performed. This study set out to determine the overall sensitivity, taking into account the optical losses and the ring resonator sensitivity. It turns out that the slot waveguide-based ring resonator has a higher overall sensitivity than most traditional ring resonator sensors based on strip waveguides. Thus, it appears to be promising for a wide range of sensing applications, including biochemical sensors.

Author details

Patrick Steglich

Address all correspondence to: patrick.steglich@th-wildau.de

Technical University of Applied Sciences Wildau, Germany

References

[1] Almeida VR, Xu Q, Barrios CA, Lipson M. Guiding and confining light in void nanostructure. Optics Letters. 2004;**29**(11):1209-1211. DOI: 10.1364/OL.29.001209

[2] Leuthold J, Koos C, Freude W, Alloatti L, Palmer R, Korn D, Pfeifle J, Lauermann M, Dinu R, Wehrli S, Jazbinsek M, Gunter P, Waldow M, Wahlbrink T, Bolten J, Kurz H, Fournier M, Fedeli J-M, Yu H, Bogaerts W. Silicon-organic hybrid electro-optical devices. Selected Topics in Quantum Electronics. 2013;**19**(6):114-126. DOI: 10.1109/JSTQE.2013.2271846

[3] Alloatti L, Palmer R, Diebold S, Pahl KP, Chen B, Dinu R, Fournier M, Fedeli J-M, Zwick T, Freude W, Koos C, Leuthold J. 100 GHz silicon-organic hybrid modulator. Light: Science and Applications. 2014;**3**(5):e173. DOI: 10.1038/lsa.2014.54

[4] Kong M, Jiang Y. Transverse magnetic modes in planar slot waveguides. Journal of the Optical Society of America B: Optical Physics. 2015;**32**(10):2052-2060. DOI: https://doi.org/10.1364/JOSAB.32.002052

[5] Chrostowski L, Hochberg M. Silicon Photonics Design: From Devices to Systems. 1st ed. Cambride: Cambridge University Press; 2015

[6] Baehr-Jones T, Hochberg M, Walker C, Scherer A. High-q optical resonators in silicon-on-insulator-based slot waveguides. Applied Physics Letters. 2005;**86**(8):081101. DOI: http://dx.doi.org/10.1063/1.1871360

[7] Vivien L, Pavesi L. Handbook of Silicon Photonics. 1st ed. Boca Raton: Taylor & Francis; 2013. 835 p

[8] Claes T, Molera JG, De Vos K, Schacht E, Baets R, Bienstman P. Label-free biosensing with a slot-waveguide-based ring resonator in silicon on insulator. IEEE Photonics Journal. 2009;**1**(3):197-204. DOI: 10.1109/JPHOT.2009.2031596

[9] Larry R. Dalton, Peter Günter, Mojca Jazbinsek, O-Pil Kwon, Philip A. Sullivan. Organic Electro-Optics and Photonics: Molecules, Polymers and Crystals. 1st ed. Cambridge University Press; 2015. 300 p

[10] Yesodha SK, Pillai CKS, Tsutsumi N. Stable polymeric materials for nonlinear optics: A review based on azobenzene systems. Progress in Polymer Science. 2004;**29**(1):45-74

[11] Steglich P, Mai C, Stolarek D, Lischke S, Kupijai S, Villringer C, Pulwer S, Heinrich F, Bauer J, Meister S, Knoll D, Casalboni M, Schrader S. Novel ring resonator combining strong field confinement with high optical quality factor. IEEE Photonics Technology Letters. 2015;**27**(20):2197-2200. DOI: 10.1109/LPT.2015.2456133

[12] Steglich P, Mai C, Stolarek D, Lischke S, Kupijai S, Villringer C, Pulwer S, Heinrich F, Bauer J, Meister S, Knoll D, Casalboni M, Schrader S. Partially slotted silicon ring resonator covered with electro-optical polymer. Proceedings of SPIE. 2016;**9891**(98910R):98910R-98910R-7. DOI: 10.1117/12.2217725

[13] Steglich P, Villringer C, Pulwer S, Casalboni M, Schrader S. Design optimization of silicon-on-insulator slot-waveguides for electro-optical modulators and biosensors. In: Ribeiro P, Raposo M, editors. Photoptics 2015. 1st ed. Cham: Springer International Publishing; 2016. pp. 173-187. DOI: 10.1007/978-3-319-30137-2_11

[14] Sun Y, Fan X. Optical ring resonators for biochemical and chemical sensing. Analytical and Bioanalytical Chemistry. 2011;**399**(1):205-211. DOI: 10.1007/s00216-010-4237-z

[15] Steglich P, Villringer C, Dümecke S, Michel YP, Casalboni M, Schrader S. Silicon-on-insulator slot-waveguide design trade-offs. In: Ribeiro P, Raposo M, editors. International Conference on Photonics, Optics and Laser Technology; Berlin. IEEE; 2015. pp. 47-52. DOI: http://ieeexplore.ieee.org/stamp/stamp.jsp?tp=&arnumber=7513125&isnumber=7513093

[16] Malitson IH. Interspecimen comparison of the refractive index of fused silica. Journal of the Optical Society of America. 1965;**55**:1205-1209. DOI: 10.1364/JOSA.55.001205

[17] Salzberg CD, Villa JJ. Infrared refractive indexes of silicon germanium and modified selenium glass. Journal of the Optical Society of America. 1957;**47**(3):244-246. DOI: 10.1364/JOSA.47.000244

[18] Korn D, Palmer R, Yu H, Schindler PC, Alloatti L, Baier M, Schmogrow R, Bogaerts W, Selvaraja SK, Lepage G, Pantouvaki M, Wouters JMD, Verheyen P, Van Campenhout J, Chen B, Baets R, Absil P, Dinu R, Koos C, Freude W, Leuthold J. Silicon-organic hybrid (SOH) IQ modulator using the linear electro-optic effect for transmitting 16QAM at 112 Gbit/s. Optics Express. 2013;**21**(11):13219-13227. DOI: 10.1364/OE.21.013219

[19] Palmer R, Alloatti L, Korn D, Schindler PC, Baier M, Bolten J, Wahlbrink T, Waldow M, Dinu R, Freude W, Koos C, Leuthold J. Low power Mach-Zehnder modulator in silicon-organic hybrid technology. IEEE Photonics Technology Letters. 2013;**25**(13):1226-1229. DOI: 10.1109/LPT.2013.2260858

[20] Palmer R, Alloatti L, Korn D, Schindler PC, Schmogrow R, Heni W, Koenig S, Bolten J, Wahlbrink T, Waldow M, Yu H, Bogaerts W, Verheyen P, Lepage G, Pantouvaki M, Van Campenhout J, Absil P, Dinu R, Freude W, Koos C, Leuthold J. Silicon-organic hybrid MZI modulator generating OOK, BPSK and 8-ASK signals for up to 84 Gbit/s. IEEE Photonics Journal. 2013;**5**(2):6600907-6600907. DOI: 10.1109/JPHOT.2013.2258142

[21] Steglich P, Villringer C, Pulwer S, Heinrich F, Bauer J, Dietzel B, Mai C, Mai A, Casalboni M, Schrader S. Hybrid-waveguide ring resonator for biochemical sensing. IEEE Sensors Journal. 2017;**17**(15):4781-4790. DOI: 10.1109/JSEN.2017.2710318

[22] Wei T, Han Y, Li Y, Tsai H-L, Xiao H. Temperature-insensitive miniaturized fiber inline Fabry-Perot interferometer for highly sensitive refractive index measurement. Optics Express. 2008;**16**(8):5764-5769. DOI: 10.1364/OE.16.005764

[23] Sun X, Dai D, Thylén L, Wosinski L. Double-slot hybrid Plasmonic ring resonator used for optical sensors and modulators. Photonics. 2015;**2**(4):1116. DOI: 10.3390/photonics2041116

[24] Ding R, Baehr-Jones T, Kim W-J, Xiong X, Bojko R, Fedeli J-M, Fournier M, Hochberg M. Low-loss strip-loaded slot waveguides in silicon-on-insulator. Optics Express. 2010;**18**(24): 25061-25067. DOI: 10.1364/OE.18.025061

[25] Alasaarela T, Korn D, Alloatti L, Saynatjoki A, Tervonen A, Palmer R, Leuthold J, Freude W, Honkanen S. Reduced propagation loss in silicon strip and slot waveguides coated by atomic layer deposition. Optics Express. 2011;**19**(12):11529-11538. DOI: 10.1364/OE.19.011529

[26] Saynatjoki A, Karvonen L, Alasaarela T, Tu X, Liow TY, Hiltunen M, Tervonen A, Lo GQ, Honkanen S. Low-loss silicon slot waveguides and couplers fabricated with optical lithography and atomic layer deposition. Optics Express. 2011;**19**(27):26275-26282. DOI: 10.1364/OE.19.026275

[27] Zhang W, Serna S, Roux XL, Alonso-Ramos C, Vivien L, Cassan E. Analysis of silicon-on-insulator slot waveguide ring resonators targeting high Q-factors. Optics Letters. 2015; **40**(23):5566-5569. DOI: https://doi.org/10.1364/OL.40.005566